EXPERIMENTAL STUDY OF SEISMIC AND PROGRESSIVE COLLAPSE RESILIENT COMPOSITE FRAMES

W.J. Liao[1], X.Z. Lu[2], K.Q. Lin[3], L. Zhang[1]

[1] *Ph.D. candidate, Beijing Engineering Research Center of Steel and Concrete Composite Structures, Tsinghua University, Beijing, China, liaowj17@mails.tsinghua.edu.cn; zhanglei14@mails.tsinghua.edu.cn*

[2] *Professor, Key Laboratory of Civil Engineering Safety and Durability of Ministry of Education, Tsinghua University, China., luxz@tsinghua.edu.cn*

[3] *Associate professor, College of Civil Engineering, Fuzhou University, Fuzhou, China, linkq@fzu.edu.cn*

Abstract

A steel-concrete composite frame is typically used for building construction. Earthquake action and progressive collapse event caused by accidental local failures are the primary threats affecting the safety of steel-concrete composite frames. Currently, multi-hazard resistance and building resilience have garnered much research attention from the international civil engineering community. Based on the optimization outcome of the first-generation seismic and progressive collapse resistant composite frame (SPCRCF), an improved second-generation seismic and progressive collapse resilient steel-concrete composite frame (SPCRCF-2) is proposed. The frame SPCRCF comprises H-shaped steel beams connecting concrete-filled steel tube (CFST) columns through beam-column self-centering connections. The connections are composed of post-tensioning (PT) tendons, replaceable energy-dissipating components (i.e. the stiffening angle steel (SAS)), and a shear panel. Compared to the SPCRCF, SPCRCF-2 is improved in the following aspects to avoid the premature local buckling of the beams caused by the compressive arch action (CAA) in progressive collapse scenarios: (i) A 15-mm gap is reserved between the beam and column; (ii) The bolt holes in the angle steel and rib stiffeners are made elliptical shape. The purpose of this design is to release the axial force in the beams by allowing moderate slipping between the frame beam and the SAS during the CAA stage.

The performance of SPCRCF-2 is validated through both seismic and progressive collapse tests of corresponding substructures. In the seismic cyclic tests, the key components (beams and column) of SPCRCF-2 exhibited no damage, whereas the damage was found on the SAS components. In the progressive collapse tests, SPCRCF-2 exhibited the greatest ductility and safety margin. At the end of the loading, the key components (beams and column) in SPCRCF-2 were damage-free, demonstrating superior resilient performance. Therefore, the proposed new SPCRCF-2 could satisfy the seismic and progressive collapse resilience requirements and serve as a reference for future multi-hazard resilient designs of composite frames.

Keywords: multi-hazard resilience, earthquake, progressive collapse, experiment

1. Introduction

Multi-hazard resistance of structures is an important challenge in civil engineering research. Indeed, the National Science Foundation of the United States (NSF) indicated that the resistance and sustainable development of structures under multi-hazard and complex environments should be improved [1]. Previous studies reveal that earthquake actions and progressive collapse events are the primary hazardous causes that impact the structural safety of steel-concrete composite frames [2, 3]. After a long period of scientific research and engineering practice, some relatively mature design methods for seismic design and progressive collapse design of steel-concrete composite structures have been developed. However, recent studies have shown that the individual design methods for specific hazards may affect structural performance against other hazards [4, 5]. Limited work has been reported on developing new structural systems against multi-hazards. Therefore, a multi-hazard resistant structural system and the associated design method are necessary to be developed.

In recent years, the study of structural resilience has attracted increasing attention, particularly those related to structural seismic resilience. As frequently reported in the literature, pre-stressed steel strands and replaceable energy-dissipating components are used to control the damage and residual deformation of structures. By contrast, investigations on the resilience of high-performance structures or components against progressive collapse are scarce. For a frame structure under a middle column-removal scenario, owing to the compressive arch action (CAA), the axial forces in the beams are increased significantly leading to premature local buckling, thus severely affecting the structural resilience [6, 7]. Therefore, it is imperative to study how CAA-induced damages can be avoided in structures, especially in steel-concrete composite frame structures under a progressive collapse event, and simultaneously improve both seismic and progressive collapse resilience.

Based on the optimization outcome of the first-generation seismic and progressive collapse resistant steel-concrete composite frame (SPCRCF), an improved second-generation seismic and progressive collapse resilient steel-concrete composite frame (SPCRCF-2) is proposed in this work to achieve structural resilience against both seismic actions and progressive collapse events. Seismic and progressive collapse experiments on the conventional steel-concrete composite frame (CSCCF), the SPCRCF, and the SPCRCF-2 specimens were performed, and the resilience of these three structures is compared.

2. Seismic and progressive collapse resilient composite frame

2.1 Concept of SPCRCF

SPCRCF was proposed initially by Lu et al. [8] based on a conventional steel-concrete composite frame (Figure 1a). The corresponding specimens are design based on the prototype of a real 51-story frame-core tube tall building [8]. It comprises H-shaped steel beams connecting concrete-filled steel tube (CFST) columns through beam-column self-centering connections, as shown in Figure 1a. The connections are composed of post-tensioning (PT) tendons and replaceable energy-dissipating (ED) components. The PT tendon helps to minimize the structural residual deformations after a hazard through its self-centering characteristic. The stiffening angle steel (SAS), composed of angle steel and rib stiffeners, developed by Lu et al. [9] is used as the replaceable components, as shown in Figure 1a. The SASs are connected to the CFST column and the steel beam by high-strength bolts [8, 10]. Moreover, a shear panel is used for the assembly of the connection as shown in Figure 1a. These high-performance components are working together to improve both seismic and progressive collapse resistance of frame structures: (1) the SASs help to dissipate the seismic input energy; (2) the progressive collapse resistance is provided by the SASs and the PT tendons; (3) the shear panel is designed to accommodate large deformations and help the assembly of different components. More details and characteristics of SPCRCF can be referred to the experimental tests of Lu et al [8].

2.1 Concept of SPCRCF-2

2i-0069

When SPCRCF is subjected to a middle column removal, owing to the CAA, the axial forces in the beams increase significantly, leading to premature local buckling of the steel beam [8], thus significantly reducing the structural progressive collapse resilience (i.e., repairability). To avoid this undesirable phenomenon, the SPCRCF is further optimized, resulting in the SPCRCF-2 with an amended beam-column connection shown in Figure 1b. Compared with the SPCRCF, SPCRCF-2 is improved in the following aspects: (i) A 15-mm gap is reserved between the beam and column. (ii) The bolt holes in the angle steel and rib stiffeners are made elliptical shape. The purpose of this design is to release the axial force in the beams by allowing moderate slipping between the frame beam and the SAS during the CAA stage. The friction force between the frame beam and the SAS is controlled by adjusting the bolt pre-stress to keep the beams elastic before slipping of the bolted connection, thereby achieving seismic and progressive collapse resilience. (iii) Additionally, the beam section is increased slightly to ensure that the beams are free from damage.
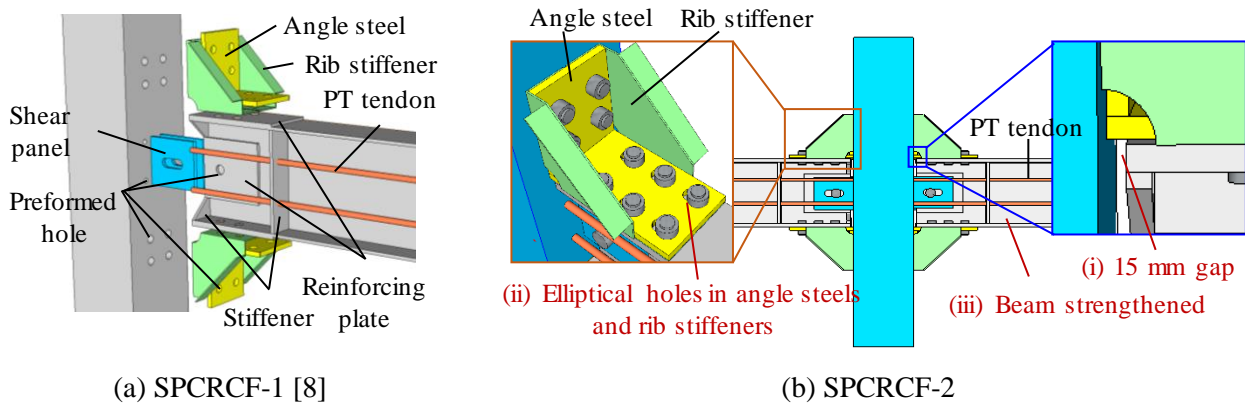

(a) SPCRCF-1 [8]   (b) SPCRCF-2

Figure 1. Concept of the SPCRCF-1 and SPCRCF-2

3. Experimental design

3.1 Design of the specimens and loading setup

The design flowchart for all the specimens is depicted in Figure 2. The experimental results of Specimens B-S, B-C, M-P100-S and M-P100-C are introduced in the previous work [8]. And the other three of the specimens (denoted as M-P140-S1.5, M-P140-S2, M-P140-C2) for the new SPCRCF-2 will be elaborated in this study.
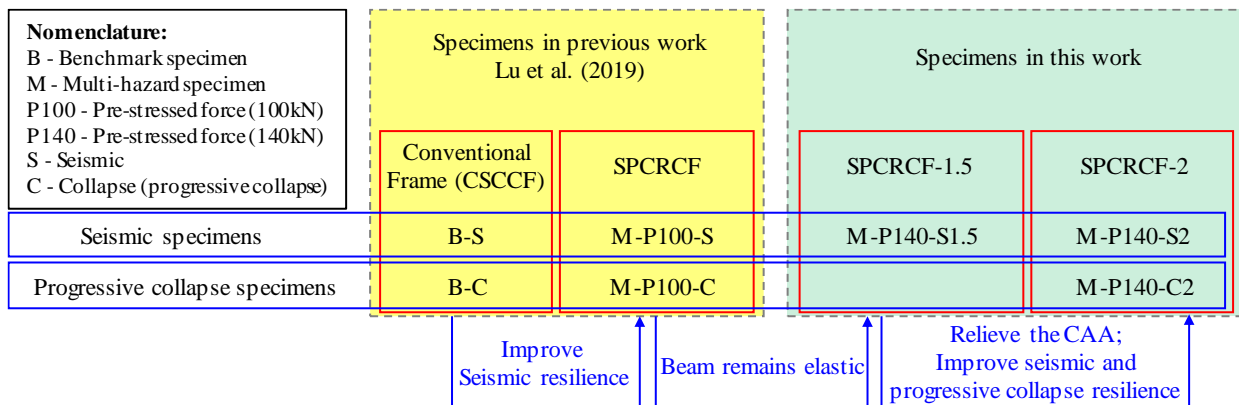

Figure 2. Design notion of the test specimens

3

In order to determine a suitable beam sectional dimension for Specimen M-P140-S2, the Specimen M-P140-S1.5 is designed to ensure that the frame beam remains in the elastic stage during the loading. Specimen M-P140-S1.5 was improved on the basis of Specimen M-P100-S. The differences between the two specimens are: (i) The beam sections of Specimen M-P140-S1.5 are strengthened; (ii) the initial pre-stressed level of the PT tendons of Specimen M-P140-S1.5 is improved (from 40% to 52%).

Specimens M-P140-S1.5 and M-P140-S2 were subjected to cyclic loads to evaluate their seismic performance. The corresponding test apparatus is shown in Figure 3a. In the seismic cyclic tests, a constant axial load of 1160 kN was applied vertically at the top of the column for considering the gravity load from the upper stories (Figure 3a). The seismic action is simulated by the cyclic loads at both ends of the beams. The rotation of the beam-column joint (i.e., θ) is calculated by $\theta = \Delta / L$, where Δ is the displacement measured at the beam end and L is the length of the beam. Note that the flexural strength deterioration shall be smaller than 20 % when θ equals 0.04 rad for a composite-special moment frame according to AISC-341-16 [11]. The cyclic loads were measured by the load cells installed at the loading actuators. The internal forces of the PT tendons were monitored by the load cells at the anchorage areas. Moreover, a series of strain gauges were installed on the angle steels and the rib stiffeners and along the beam height to monitor the strain development of different components.

On the other hand, Specimen M-P140-C2, being a two-bay substructure, was subjected to a vertical concentrated load to mimic a middle column removal scenario as shown in Figure 3b. In order to consider the constraint from the peripheral structure, both end columns of Specimen M-P140-C2 were mounted to the steel reaction frame to achieve fix boundaries. The external load was measured by the load cell above the middle column stub. Similar to the seismic cyclic tests, the strain developments and PT tendon forces were also monitored by corresponding instruments. More information about the test setups can be referred to Lu et al. [8].
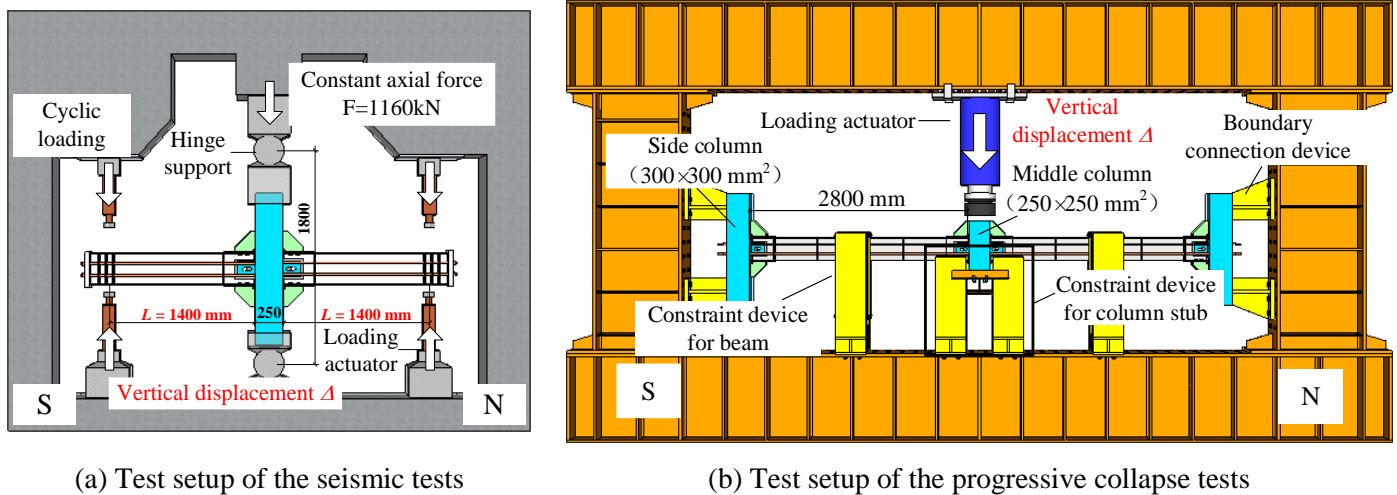

(a) Test setup of the seismic tests   (b) Test setup of the progressive collapse tests

Figure 3. Test setup

3.2 Details of the specimens

The details of Specimens M-P140-S2 and M-P140-C2 are shown in Figures 4a and 5, respectively. The progressive collapse test specimen is of identical dimensions to those of the seismic test specimens at the beam-to-column connection area (Figure 4), therefore similar dimensions are unlabeled in Figure 5. In order to balance the residual bending moment of the replaceable SAS when θ equals 0.04 rad, the initial pre-stress level was set as 52% (i.e., the initial pre-stressed force of a single PT tendon was 140 kN). The details of the SAS in Specimens M-P140-S2 and M-P140-C2 are shown in Figures 4b and 4c.

4
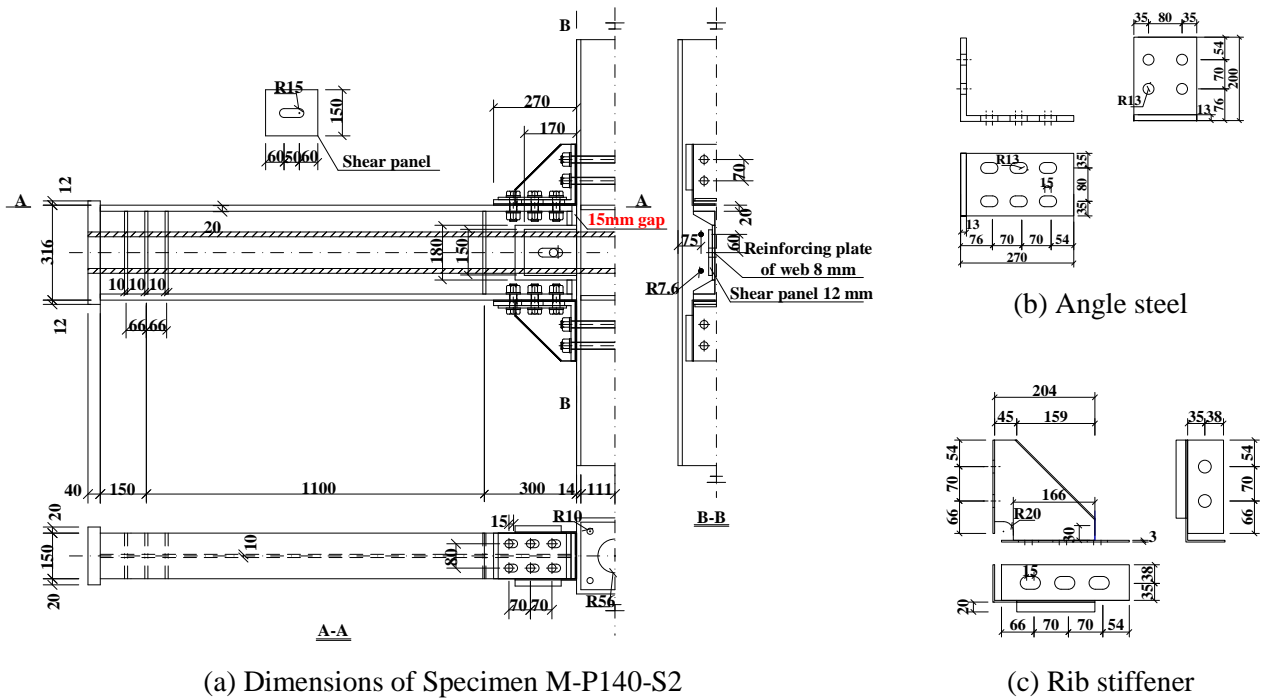
(a) Dimensions of Specimen M-P140-S2

(b) Angle steel

(c) Rib stiffener

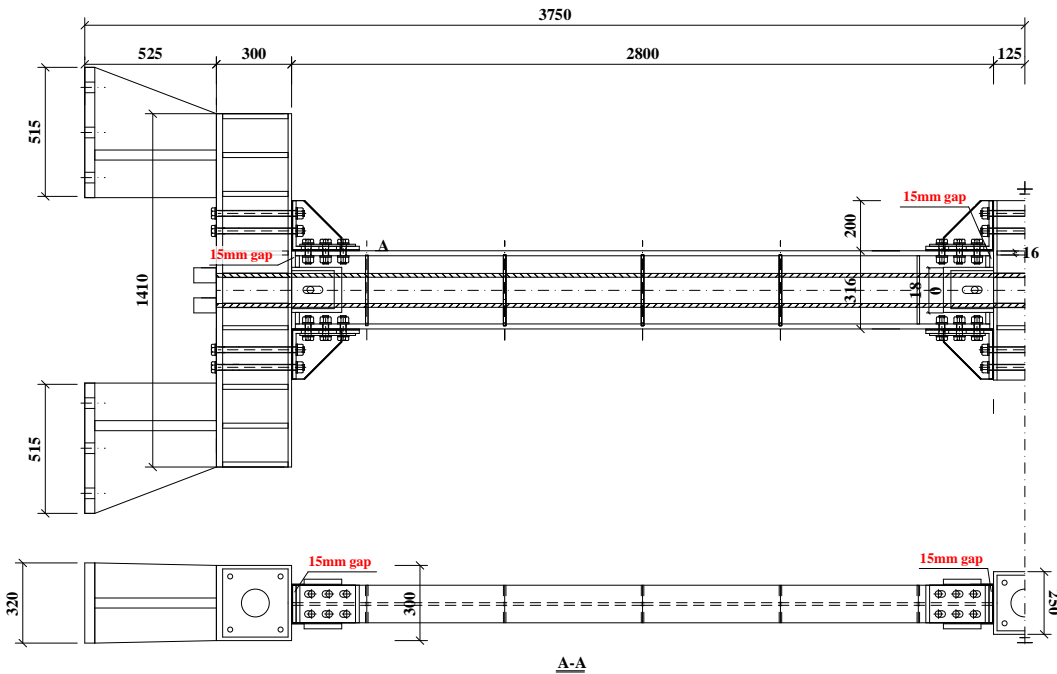Figure 4. Dimensions of Specimen M-P140-S2 and stiffening angle steel (units: mm)

Figure 5. Dimensions of Specimen M-P140-C2 (units: mm)

3.3 Material properties

The measured material properties of various steel components making up the beam-to-column connections are summarized in Table 1. The results for the steel components were derived based on the standard coupon tests as regulated in the Chinese code [12]. The 28-day concrete compressive strength of the CFST column

was 61.05 MPa based on the standard cube (150 mm $\times$ 150 mm $\times$ 150 mm) compressive tests. The nominal diameter and effective cross-section area of the PT tendons were 15.2 mm and 140 mm^2, respectively. The ultimate strength and tensile force of the PT tendons were 1933 MPa and 270.8 kN, respectively.

Table 1 – Material properties of the steel plates

Type	Thickness (mm)	Yield strength (MPa)	Ultimate strength (MPa)	Elongation
Square steel tube and conventional frame shear panel	14	359	545	35%
Shear panel (MHRSCCF-1/1.5/2)	12	403	539	33%
Flange of beam (Conventional frame and MHRSCCF-1)	9	381	506	37%
Web of beam (Conventional frame and MHRSCCF-1)	6.5	399	537	32%
Flange of beam (MHRSCCF-1.5/2)	20	369	503	25%
Web of beam (MHRSCCF-1.5/2)	10	428	588	30%
Angle steel	13	393	569	38%
Rib stiffener	3	377	513	30%

4. Experimental results

4.1 Seismic cyclic tests

The purpose of Specimen M-P140-S1.5 is to validate that the beam section size is suitable for the use in Specimen M-P140-S2, and to ensure that the frame beam remains elastic during the loading, thereby improving the structural seismic and progressive collapse resilience. The load-rotation relationship of Specimen M-P140-S1.5 is shown in Figures 6. The experimental results indicate no damage in the key components (beams and columns), whereas the damage is concentrated on the SAS components, which is deemed to satisfy the structural resilience. Therefore, the test was terminated when the rotation was greater than 2% (the maximum rotation specified in Chinese code [13]). The size of the beams in Specimen M-P140-S1.5 is confirmed to be satisfactory when used in the design of the beams in Specimen M-P140-S2.

The maximum displacement at the beam ends of Specimen M-P140-S2 was 76.4 mm, corresponding to a joint rotation of 0.055 rad. No damage was found in the beams and the column. The load-rotation relationship of this specimen is shown in Figure 7. The key reference points (i.e., A to C) associated with the hysteretic behavior in Figure 7 are linked to Figure 8. The rib stiffeners exhibited visible deformation at $\theta = 0.023$ rad (Figure 8b). Notably, the rib stiffeners ruptured at $\theta = 0.045$ rad (Figure 8c). In the next stage of the loading, the angle steel under the south beam ruptured and its strength could not continue to increase. Consequently, the loading process was ended.
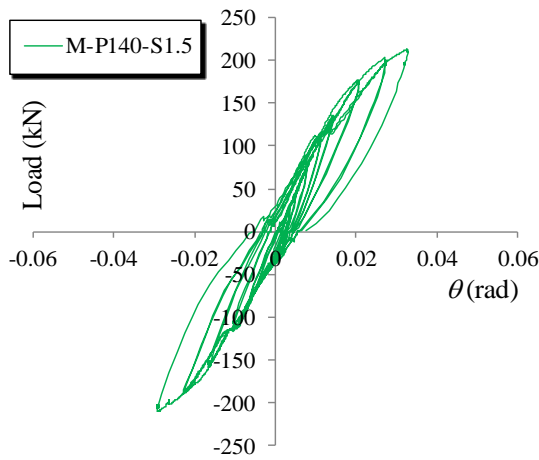
Figure 6. Load-rotation angle curve of Specimen M-P140-S1.5

A: Rib stiffener exhibited visible deformation
B: Rib stiffener ruptured
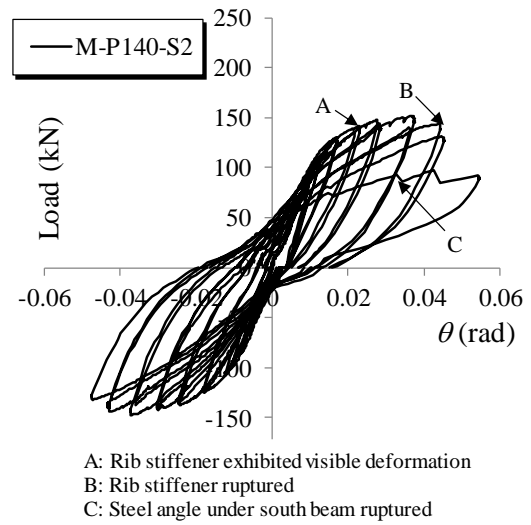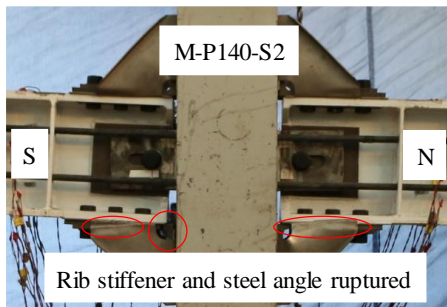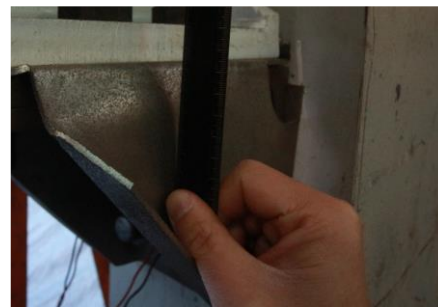C: Steel angle under south beam ruptured

Figure 7. Load-rotation angle curve of Specimen M-P140-S2

(a) Failure mode of the specimen

(b) Rib stiffener exhibited visible deformation
(A, $\theta = 0.023$ rad)

(c) Rib stiffener ruptured (B, $\theta = 0.045$ rad)

(d) Angle steel under south beam ruptured (C, $\theta = 0.033$ rad)

Figure 8. Damage progression of Specimen M-P140-S2 (Points A to C refer to Figure 7)

The backbone curves and hysteretic curves of Specimens B-S, M-P140-S1, M-P140-S2 are compared, as shown in Figure 9. The results indicate that the initial stiffness of the three specimens is similar, while the flexural yield strength of Specimen M-P140-S2 is slightly lower than that of the other specimens. This is due to the 15-mm gap between the beam and the column in Specimen M-P140-S2, which will reduce the stiffness provided by the angle steel. According to FEMA P-58 [14], a structure is repairable when its residual story drift ratio is less than 0.5%. Hence, Specimen B-S is unrepairable when the joint rotation

7

exceeds 0.019 rad according to Figure 9b. As for the other two specimens, the critical joint rotations are 0.028 rad and 0.029 rad for Specimens M-P100-S and M-P140-S2, respectively. Thus, the deformation capacities of SPCRCF and SPCRCF-2 are increased by 47.4% and 52.6%, compared to the CSCCF if the residual deformations are considered as the performance criteria. Note that a drift ratio of 0.028 rad meets the requirement of the story drift ratio limit as specified ASCE 7-16 (Table 12.12-1) [15]. Furthermore, no damage was found in the key components (beams and columns) when θ reached 0.04 rad. It can be concluded that the SPCRCF and SPCRCF-2 exhibit significantly higher seismic resilience than the CSCCF.
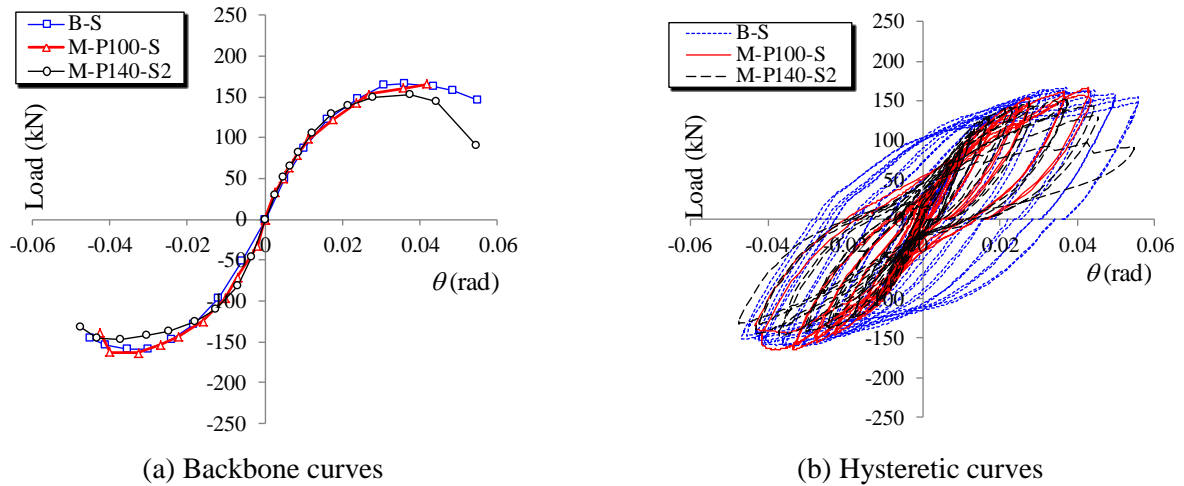

(a) Backbone curves

(b) Hysteretic curves

Figure 9. Comparison of seismic tests

4.2 Progressive collapse tests

In the progressive collapse test of Specimen M-P140-C2, the displacement of the middle column stub reached 572 mm, corresponding to a chord rotation of 0.204 rad, which is greater than the required chord rotation capacity as regulated in DoD 2016 [16]. The final deformation of Specimens M-P140-C2 are shown in Figures 10. Compared to the results of Specimens B-C and M-P100-C from the previous experiments [8], it is obvious that Specimen M-P140-C2 exhibits better deformation capacity and more effective catenary action.
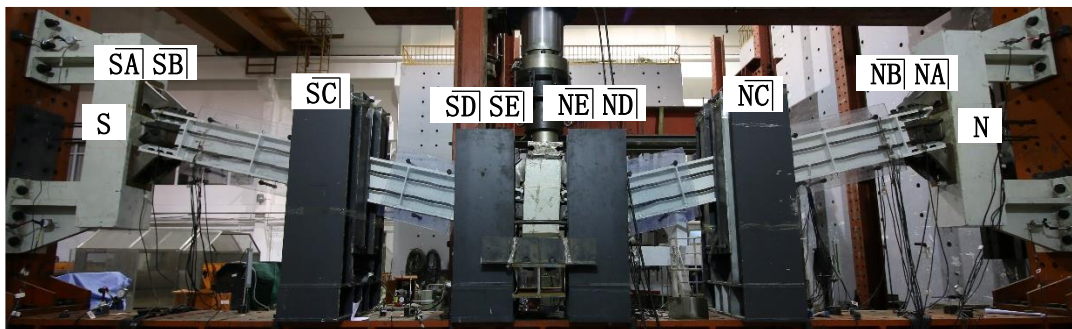

Figure 10. Overall deformation of Specimen M-P140-C2 after the test

Figure 11 depicts the load-displacement curve recorded at the column stub of Specimen M-P140-C2. Correspondingly, the experimental observations of the characteristic points marked on the curve are shown in Figure 12.

(1)   When Δ = 53 mm, the bolts slipped at Section NE (Figure 12a). The axial force of the beam was released, and the CAA was relieved.

8

(2)   When Δ = 115 mm, the tension rib stiffeners began to rupture (Figure 12b). The specimen was in the transition stage from the beam mechanism to the catenary mechanism. The resistance increased steadily.

(3)   When Δ = 372 mm, the top angle ruptured at Section SA (Figure 12c). The resistance decreased slightly (from 487 kN to 445 kN).

(4)   When Δ = 389 mm, the PT tendons began to break, and the steel wires of the PT tendons ruptured individually (Figure 12d). The resistance dropped from 486 kN to 373 kN and then rose again due to the catenary action.

(5)   When Δ = 451 mm, the bottom angle ruptured at Section NE (Figure 12e). The resistance decreased from 348 kN to 218 kN and then rose again.

(6)   When Δ = 496 mm, the top angle ruptured at Section NA (Figure 12f). The resistance dropped from 327 kN to 237 kN.

(7)   When Δ = 566 mm, the PT tendons at different positions were broken (Figure 12g). The resistance decreased significantly (from 384 kN). For safety of the experiment, the loading process was terminated.
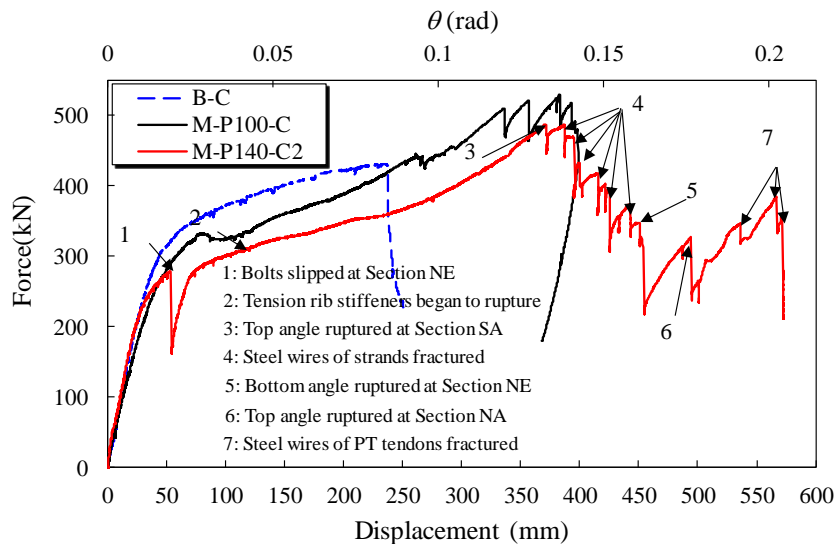

Figure 11. Load (F)-displacement (Δ) relationship of the progressive collapse tests

Compared to the CSCCF specimen (i.e., Specimen B-C), the chord rotational capacity and the load resistance of the new Specimen M-P140-C2 were 126.4% and 13.4% higher, respectively. The deformation capacity of Specimen M-P140-C2 was also 43.4% greater than Specimen M-P100-C.

It should be noted that although there were some load drops after Δ = 372 mm, the strength of this specimen was still higher than its yield strength when the rotation angle of Specimen M-P140-C2 reached 0.2 rad. The primary reason is that even some of the angle steels, rib stiffeners, and PT tendons were damaged due to large deformation, the remaining intact components still contributed significantly to the catenary resistance. Similar load drops are commonly observed in the progressive collapse tests when some reinforcement is ruptured, or the connections are damaged [17, 18, 19]. Moreover, Specimen M-P140-C2 was the only one of the three specimens that met the chord rotational capacity as regulated in DoD 2016 [16]. This specimen exhibits a larger ductility and safety margin compared with Specimen M-P140-C. Additionally, at the end of the loading, the key components (beams and columns) of Specimen M-P140-C2 were found undamaged, which facilitates the rapid recovery of the structural performance after hazardous events. Therefore, Specimen M-P140-C2 is considered to be progressive collapse resilient under column removal scenarios.

9

To sum up, SPCRCF-2 demonstrates better seismic and progressive collapse resilience when both the seismic cyclic test results (Section 4.1) and the progressive collapse test results are considered.
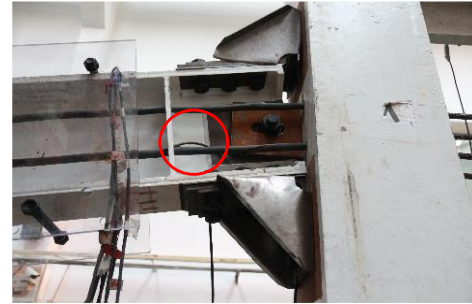
Gap became smaller
& bolts slipped
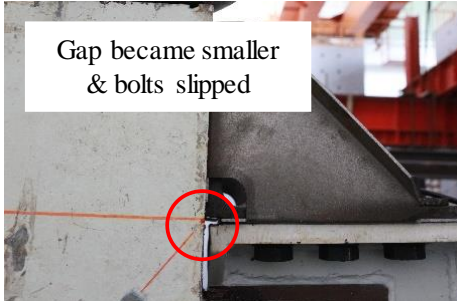
(a) Bolts slipped at Section NE
(1, Δ = 53 mm, F = 278 kN)

(b) Tension rib stiffeners began to rupture
(2, Δ = 115 mm, F = 309 kN)

(c) Top angle ruptured at Section SA
(3, Δ = 372 mm, F = 487 kN)

(d) Steel wires of a PT tendon fractured
(4, Δ = 389 mm, F = 486 kN)

(e) Bottom angle ruptured at Section NE
(5, Δ = 451 mm, F = 348 kN)

(f) Top angle ruptured at Section NA
(6, Δ = 496 mm, F = 327 kN)

10

(g) Steel wires of PT tendons fractured
(7, $\Delta = 566$ mm, $F = 384$ kN)

Figure 12. Typical phenomena of Specimen M-P140-C2 (Points 1 to 7 refer to Figure 11)

5. Conclusions

In order to improve the seismic and progressive collapse resilience of composite frames, a new composite frame system, namely, SPCRCF-2, is proposed in this study. The performance of SPCRCF-2 is compared with that of the SPCRCF and the CSCCF through seismic and progressive collapse experiments. The primary conclusions are drawn below.

(1) In the seismic tests, Specimen M-P140-S2 could provide similar initial stiffness and yield strength as those of Specimens B-S and M-P100-S. Compared with the conventional frames, the beams and columns in Specimens M-P100-S and M-P140-S2 exhibited no damages, whereas the damage was found on the replaceable SAS components. Consequently, both SPCRCF and SPCRCF-2 exhibited significantly better seismic resilience than conventional frames (CSCCF).

(2) In the progressive collapse tests, the peak strength and ductility of Specimens M-P100-C and M-P140-C2 were higher than those of Specimen B-C. Furthermore, Specimen M-P140-C2 exhibited greater ductility and safety margin compared with Specimen M-P140-C. Additionally, at the end of loading, the key components (beams and columns) of Specimen M-P140-C2 were damage-free. Therefore, SPCRCF-2 exhibited better progressive collapse resilience.

In summary, the proposed new and improved SPCRCF-2 satisfies the seismic and progressive collapse resilience requirements (i.e., large rotation, low damage, self-centering, and easy reparability), and can serve as a reference for future multi-hazard resilient designs of composite frames.

6. Acknowledgements

7. References

[1] National Science Foundation (NSF) (2014): Decision frameworks for multi-hazard resilient and sustainable buildings (RSB).

[2] Nethercot D, Vidalis C (2015): Improving the resistance to progressive collapse of steel and composite moment frames. *Structures Congress*, 1138-1149.

[3] Hajjar JF, Leon RT, Gustafson MA, Shield CK (1998): Seismic response of composite moment-resisting connections. II: behavior. *Journal of Structural Engineering*, **124** (8), 868-876.

[4] Lin KQ, Li Y, Lu XZ, Guan H (2017): Effects of seismic and progressive collapse designs on the vulnerability of RC frame structures. *Journal of Performance of Constructed Facilities*, **31** (1), 04016079.

[5] Li Y, Ahuja A, Padgett JE (2011): Review of methods to assess, design for, and mitigate multiple hazards. *Journal of Performance of Constructed Facilities*, **26** (1), 104-117.

[6] Pirmoz A (2011): Performance of bolted angle connections in progressive collapse of steel frames. *Structural Design of Tall and Special Buildings*, **20** (3), 349-370.

[7] Izzuddin BA, Vlassis AG, Elghazouli AY, Nethercot DA (2008): Progressive collapse of multi-storey buildings due to sudden column loss—Part I: Simplified assessment framework. *Engineering Structures*, **30** (5), 1308-1318.

[8] Lu XZ, Zhang L, Lin KQ, Li Y (2019): Improvement to composite frame systems for seismic and progressive collapse resistance. *Engineering Structures*, **186**, 227-242.

[9] Lu XZ, Zhang L, Cui Y, Li Y, Ye LP (2018): Experimental and theoretical study on a novel dual-functional replaceable stiffening angle steel component. *Soil Dynamics and Earthquake Engineering*, **114**, 378-391.

[10] Lu XL, Cui Y, Liu JJ, Gao WJ (2015): Shaking table test and numerical simulation of a 1/2‐scale self‐centering reinforced concrete frame. *Earthquake Engineering & Structural Dynamics*, **44** (12), 1899-1917.

[11] American Institute of Steel Construction (AISC) (2016): *Seismic Provisions for Structural Steel Buildings*. ANSI/AISC 341-16, Chicago.

[12] Standardization Administration of the People's Republic of China (SAC) (2010): *Metallic Materials - Tensile Testing - Part l: Method of Test at Room Temperature* (GB/T 228.1 - 2010). Beijing: China Zhijian Publishing House. (in Chinese)

[13] Ministry of Housing and Urban-Rural Development of the People's Republic of China (MOHURD) (2010): *Code for Seismic Design of Buildings* (GB50011-2010). Beijing: China Architecture & Building Press. (in Chinese).

[14] Federal Emergency Management Agency (FEMA) (2012): *Seismic Performance Assessment of Buildings Volume 1-Methodology*, FEMA P-58. Federal Emergency Management Agency, Washington, D.C.

[15] American Society of Civil Engineers (ASCE) (2016): *Minimum Design Loads and Associated Criteria for Buildings and Other Structures*. ASCE/SEI 7-16, Reston, VA.

[16] Department of Defense (DoD) (2016): *Design of Structures to Resist Progressive Collapse* (Change 3). Unified Facility Criteria, UFC 4-023-03, Washington, D.C.

[17] Yu J, Tan KH (2013): Structural behavior of RC beam-column subassemblages under a middle column removal scenario. *Journal of Structural Engineering*, **139** (2), 233-250.

[18] Yang B, Tan KH (2013): Robustness of bolted-angle connections against progressive collapse: Experimental tests of beam-column joints and development of component-based models. *Journal of Structural Engineering*, **139** (9), 1498-1514.

[19] Li L, Wang W, Chen YY, Lu Y (2013): Experimental investigation of beam-to-tubular column moment connections under column removal scenario. *Journal of Constructional Steel Research*, **88**, 244-255.

12